Front. Optoelectron. 2020, 13(2): 139–148
https://doi.org/10.1007/s12200-020-1018-y

RESEARCH ARTICLE

Highly stable and repeatable femtosecond soliton pulse generation from saturable absorbers based on two-dimensional $Cu_{3-x}P$ nanocrystals

Haoran MU[1], Zeke LIU[2], Xiaozhi BAO[3], Zhichen WAN[1], Guanyu LIU (✉)[4], Xiangping LI[4], Huaiyu SHAO[3], Guichuan XING[3], Babar SHABBIR[1], Lei LI[5], Tian SUN[2], Shaojuan LI[2], Wanli MA[2], Qiaoliang BAO (✉)[1]

1 Department of Materials Science and Engineering and ARC Centre of Excellence in Future Low-Energy Electronics Technologies (FLEET), Monash University, Clayton, Victoria 3800, Australia
2 Institute of Functional Nano and Soft Materials (FUNSOM), Jiangsu Key Laboratory for Carbon-Based Functional Materials and Devices, and Collaborative Innovation Center of Suzhou Nano Science and Technology, Soochow University, Suzhou 215123, China
3 Joint Key Laboratory of the Ministry of Education, Institute of Applied Physics and Materials Engineering (IAPME), University of Macau, Macau, China
4 Guangdong Provincial Key Laboratory of Optical Fiber Sensing and Communications, Institute of Photonics Technology, Jinan University, Guangzhou 510632, China
5 Jiangsu Key Laboratory of Advanced Laser Materials and Devices, Jiangsu Collaborative Innovation Center of Advanced Laser Technology and Emerging Industry, School of Physics and Electronic Engineering, Jiangsu Normal University, Xuzhou 221116, China

Abstract Heavily doped colloidal plasmonic nanocrystals have attracted great attention because of their lower and adjustable free carrier densities and tunable localized surface plasmonic resonance bands in the spectral range from near-infra to mid-infra wavelengths. With its plasmon-enhanced optical nonlinearity, this new family of plasmonic materials shows a huge potential for nonlinear optical applications, such as ultrafast switching, nonlinear sensing, and pulse laser generation. $Cu_{3-x}P$ nanocrystals were previously shown to have a strong saturable absorption at the plasmonic resonance, which enabled high-energy Q-switched fiber lasers with 6.1 μs pulse duration. This work demonstrates that both high-quality mode-locked and Q-switched pulses at 1560 nm can be generated by evanescently incorporating two-dimensional (2D) $Cu_{3-x}P$ nanocrystals onto a D-shaped optical fiber as an effective saturable absorber. The 3 dB bandwidth of the mode-locking optical spectrum is as broad as 7.3 nm, and the corresponding pulse duration can reach 423 fs. The repetition rate of the Q-switching pulses is higher than 80 kHz. Moreover, the largest pulse energy is more than 120 μJ. Note that laser characteristics are highly stable and repeatable based on the results of over 20 devices. This work may trigger further investigations on heavily doped plasmonic 2D nanocrystals as a next-generation, inexpensive, and solution-processed element for fascinating photonics and optoelectronics applications.

Keywords plasmonic semiconductors, fiber laser, mode-locking, ultrafast generation

1 Introduction

Passively mode-locked fiber lasers are used in a wide range of applications in different fields, including fiber communications, material machining, and medical surgery, because of their simple and compact structure, excellent light beam quality, high cost-effectiveness, and good compatibility to fiber optical systems [1,2]. Nonlinear optical materials, called saturable absorbers (SAs), must be inserted into the laser system without any additional mechanical or electrical modulation to realize the passive mode-locking operation [2]. The longitude mode of the laser would be locked, and the output pulses would be compressed at the sub-picosecond level because of the selective absorption between the strong and weak lights of the SA. Bulk materials generally have a weak optical nonlinearity, which hardly meets practical mode-locking requirements; therefore, semiconductor quantum wells, called semiconductor saturable absorber mirrors, were

Received February 27, 2020; accepted June 5, 2020

E-mails: liuguanyu@jnu.edu.cn (G. Liu), qiaoliang.bao@gmail.com (Q. Bao)

developed [3]. However, these semiconductor quantum wells had many drawbacks, such as complex and expensive fabrication processes. In the recent years, different low-dimensional nanomaterials with inherent quantum confinement effects and large optical nonlinearities have achieved excellent mode-locking performances [4–8]. For example, a graphene-based mode-locked fiber laser with an ultra-compact laser cavity (~1 cm) generated subpicosecond pulses [9], while both WS_2 and black phosphorus achieved a sub-150 fs pulse generation in fiber laser systems [10,11]. Various nanomaterials, such as MXene [12], perovskite [13], two-dimensional (2D) TiS_2 [14], bismuthine [15], and antimonene [16], are applied in ultrafast lasers. However, nanomaterial-based saturable absorption devices still have a long way to go before entering commercial applications because most of them have low repeatability and face difficulties in scaling up.

Plasmonic semiconductor nanocrystals (NCs) show great potential for use as SAs in ultrafast photonics because of the nonlinear optical enhancement effect at the localized surface plasmonic resonance (LSPR) frequency region [17,18]. In comparison to traditional noble plasmonic metals (e.g., gold, silver, and copper), plasmonic semiconductor NCs (e.g., $Cu_{2-x}S$, $Cu_{2-x}Se$, $Cu_{2-x}Te$) [19,20] have a long LSPR wavelength of 1000 nm to 7 μm, which is caused by their lower carrier concentrations [21,22] and tunable LSPR frequency obtained by simply adjusting their element composition [23]. Self-doped colloidal copper phosphide ($Cu_{3-x}P$) nanocrystals, which are an emerging member of 2D plasmonic nanomaterials, were recently found to have an ultrafast dynamic response (~130 fs) and a strong optical nonlinearity in terms of a relatively large modulation depth ($>18\%$) [19]. Accordingly, high-energy and stable Q-switching pulses at 1.5 μm were generated by drop-casting its solution onto the end-facet of an optical fiber as a new kind of saturable absorber. $Cu_{2-x}S$ nanocrystals were also later proved to be effective saturable absorbers for mode-locking pulse generation at 1.0, 1.5, and 2.0 μm wavebands [24]. However, the LSPR peak of $Cu_{2-x}S$ nanocrystals is around 1200 nm, while that of $Cu_{3-x}P$ nanocrystals can be precisely adjusted to 1550 nm, which is more suitable for telecommunication optical applications. The advantages of semiconductor 2D NCs over other nanomaterials, especially their repeatability and potential for scalable industrial production, have not yet been fully investigated.

In this study, $Cu_{3-x}P$ nanocrystals synthesized by the "one-pot" approach were drop-casted onto D-shaped fibers as a robust saturable absorber with a strong evanescent field interaction. Both mode-locking and Q-switching pulses at 1560 nm can be generated with high stability by tuning the concentration of the 2D $Cu_{3-x}P$ nanocrystal solution. Note that all as-fabricated SA devices (i.e., over 20 devices) can generate stable mode-locking pulses with similar characteristics, indicating a good repeatability.

2 Experimental and discussion

2.1 Material preparation and characterizations

Self-doped colloidal copper phosphide ($Cu_{3-x}P$) nanocrystals were synthesized by the "one-pot" approach in solution at room temperature. All synthesis processes were performed with standard air-free Schlenk line techniques under a nitrogen atmosphere [19,25]. A solution composed of 890 mg (2.4 mmol) trioctylphosphine (TOP), 60 mg (0.6 mmol) CuCl, and 5 mL of oleylamine was degassed at 100°C in a 25 mL three-neck flask and kept under vacuum for 1 h. The solution was then heated to a desired temperature under nitrogen (60°C–180°C). Subsequently, 500 mg (0.1 mmol) tris(trimethylsilyl)phosphiphine $(TMSi)_3P$ (10 wt.% in hexane) was dissolved in 1 mL octadecene under vacuum to remove hexane. The $(TMSi)_3P$ solution was then quickly injected into the hot solution. After 3 min, the reaction was stopped by removing the heating mantle. Purification by precipitating hexane/acetone twice was performed, and the product was stored in solid form in a nitrogen-filled glove box. For the *in-situ* thermal treatment process, the abovementioned reaction must be heated to 300°C for 10 min, followed by a heating mantle removal. The purification process is the same as above. The $Cu_{3-x}P$ nanocrystal concentration chosen for the optical experiment was approximately 5 mg/L.

The as-prepared $Cu_{3-x}P$ nanocrystals were spin-coated onto the SiO_2 substrate for characterization. Figure 1 illustrates the scanning electron microscopy results. 2D nanocrystals with a hexagonal shape and a very similar size were densely arranged on the substrate. The typical crystal size was around 20.1 nm, as depicted by the inset of Fig. 1. The atomic force microscopy (AFM) image showed that the single nanocrystal thickness was approximately 2 nm, confirming its 2D nature. The optical absorption spectra were characterized as shown in Fig. 1(c), where the LSPR peak of the $Cu_{3-x}P$ nanocrystals was found around 1456 nm, to verify the LSPR effect of the $Cu_{3-x}P$ nanocrystals. When the solution was spin-coated onto the quartz substrate, the LSPR peak showed a significant redshift to 1562 nm, which was mainly caused by the Coulomb gravitational between the nearest-neighbor nanocrystals when forming the film [26]. The X-ray powder diffraction (XRD) patterns in Fig. 1(d) depict well-resolved peaks that are coincidental with Joint Committee on Powder Diffraction Standards (JSPDS) card Nos. 71-2261 and indicated a hexagonal Cu_3P structure (space group $P6_3cm$). In Fig. 1(e), the ^1H nuclear magnetic resonance (NMR) resonance peak of the TOP can be easily distinguished in

Cu_3P NCs, indicating that the TOP would chemisorb to the surface of the $Cu_{3-x}P$ NCs as ligands. The sharp resonances of 2.18 ppm (1 ppm = 10^{-6}) in Fig. 1(b) can be attributed to residual acetone. Figure 1(f) illustrates a schematic of the hexagonal Cu_3P structure with the TOP as ligands.

Accordingly, PL spectroscopy and imaging were performed (panels d–f) to further confirm that the optical absorption peak in Fig. 1(c) was induced by the LSPR effect rather than the bandgap effect. Figure 1(g) depicts the optical image of a $Cu_{3-x}P$ nanocrystal assembly. Figure 1(h) shows the corresponding PL mapping result. The $Cu_{3-x}P$ nanocrystals clearly had a strong PL emission throughout the whole assembly. Moreover, the PL peak was found around 600 nm (Fig. 1(i)), which was caused by the optical interband transition. Note that the PL peak was relatively broad mainly because the optical bandgap was very sensitive to the nanocrystal size.

2.2 Nonlinear optical properties

The $Cu_{3-x}P$ nanocrystal solution was drop-casted onto the side-polished fibers as SA devices. The evanescently interacted devices had different modulation depths and saturable intensities obtained by controlling the amount of $Cu_{3-x}P$ nanocrystals. We used the twin-detector measurement technique herein to study the nonlinear optical absorption of the $Cu_{3-x}P$ nanocrystals. The optical source was a home-made, mode-locked fiber laser with 786 fs duration and 20.6 MHz repetition rate. The maximum light intensity was over 200 MW/cm^2. The saturable absorption performance was evaluated by recording the transmission

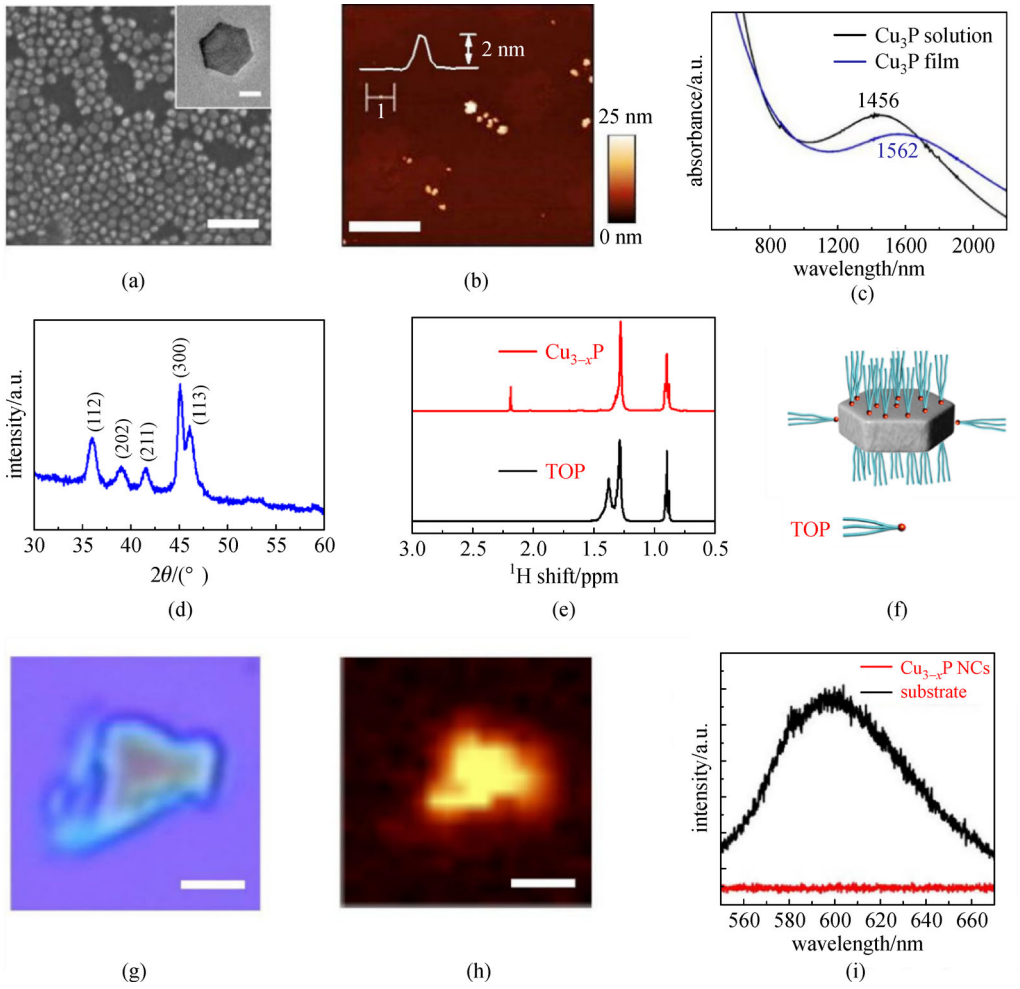

Fig. 1 Material morphology and optical characterizations of $Cu_{3-x}P$ nanocrystals. (a) SEM image of $Cu_{3-x}P$ nanocrystals (scale bar: 100 nm) and TEM image of single $Cu_{3-x}P$ NC (inset: 10 nm scale bar). (b) AFM image (scale bar: 1 μm). (c) Optical absorption spectra of $Cu_{3-x}P$ nanocrystals in toluene solution (black line) and silicon substrate (blue line). (d) Typical XRD patterns of $Cu_{3-x}P$ NCs (i.e., the well-resolved peaks overlapped well with the hexagonal Cu_3P structure (space group: $P6_3cm$). (e) ^{1}H NMR spectra of TOP (bottom) and $Cu_{3-x}P$ NCs (top) dissolved in $CDCl_3$. (f) Schematic diagram of $Cu_{3-x}P$ NCs. (g) Optical image of $Cu_{3-x}P$ nanocrystal assembly. (h) Corresponding photoluminescence (PL) mapping result (scale bar: 1 μm). (i) PL spectrum of $Cu_{3-x}P$ nanocrystal assembly

data under different incident intensities. The saturable absorption in the $Cu_{3-x}P$ nanocrystals can be fitted as follows:

$$\alpha(I) = \frac{\alpha_S}{1 + I/I_S} + \alpha_{NS},$$

where α_S is the modulation depth relevant to the nonlinear optical modulation capacity of the SA device; I_S is the saturation intensity for weighing the required optical intensity, where optical bleaching occurred; and α_{NS} is a non-saturation component.

Figure 2 shows the typical saturable absorption results of the $Cu_{3-x}P$-based SA devices. Two samples with different amounts of $Cu_{3-x}P$ nanocrystals were prepared for comparison. With the increase of the amount of $Cu_{3-x}P$ nanocrystals on the fiber, the saturation intensity slightly increased from 112.05 (Fig. 2(a)) to 125.53 MW/cm^2 (Fig. 2(b)), while the modulation depth decreased from 26.97% to 11.82%. The non-saturation component α_{NS} greatly increased from 18.57% (Fig. 2(a)) to 73.36% (Fig. 2(b)), indicating a large transmission loss of the second SA device.

2.3 $Cu_{3-x}P$ nanocrystals as saturable absorbers for ultrafast fiber lasers

The laser cavity had a typical ring configuration consisting of a 0.75 m long Erbium-doped fiber (LIKKI Er-80/125) with an absorption coefficient of 80 dB/m at 976 nm, a 980 nm/1550 nm wavelength division multiplexer (WDM), a 90:10 coupler, an isolator, and a polarization controller (PC). The polarization-independent isolator was used to force the unidirectional operation of the ring. The PC was used to adjust the intra-cavity polarization. The laser was pumped by a 980 nm laser diode with a maximum average power of 500 mW. The laser output was then extracted from 10% output port of the coupler and analyzed for mode-locking characterization.

Only a continuous wave could be observed when the brand-new side-polished fiber was inserted into the laser cavity without a $Cu_{3-x}P$ nanocrystal sample, unless the polarization state and the pump power were adjusted (Fig. S1(a)). The corresponding optical image of the side-polished fiber was posted as an inset of the figure. Drop-casting the $Cu_{3-x}P$ nanocrystal solution onto the side-polished fiber will result in the formation of a $Cu_{3-x}P$ nanocrystal thin film after drying and interacting with the intracavity light through the evanescent field effect. Interestingly, the laser output state evolved from the continuous wave to the mode-locking state with the increase of the amount of $Cu_{3-x}P$ nanocrystals from 40 to 120 μL (Figs. S1(b)–S1(f)). During this process, the pump power was maintained at 150 mW, and no other intracavity parameters were changed. The smooth optical spectrum curve in Fig. S1(f) denotes the stable mode-locking state, in which the continuous wave component was suppressed. The clear Kelly sideband suggests that the laser worked on the anomalous dispersion state, and the 3 dB bandwidth was 3.5 nm.

The cavity parameters, including cavity length, intra-cavity dispersion, and polarization states, were then carefully tuned. Figure 3 shows the representative soliton mode-locking results. The optical spectrum in Fig. 3(a) illustrates that the central working wavelength was 1570 nm with a 3 dB bandwidth of around 7.3 nm. The pulse train had a repetition of 31 MHz without a clear modulation on the top of the train, indicating the high quality of the mode-locking output (Fig. 3(b)). The single pulse envelope was fitted by the Sech^2 formula. The pulse duration was as short as 423 fs (Fig. 3(c)). The laser

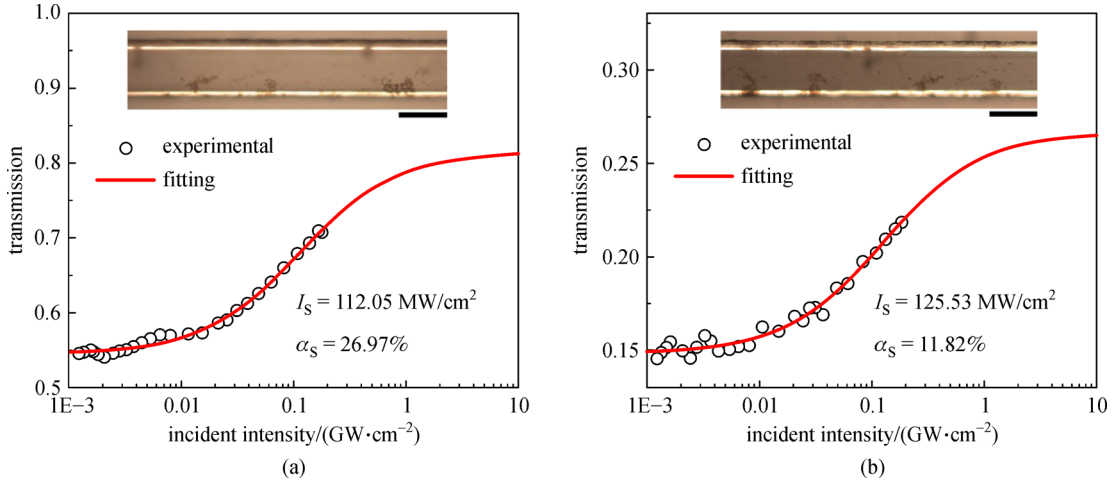

Fig. 2 Nonlinear absorption curves of the evanescently interacted $Cu_{3-x}P$ SAs measured by the balanced twin-detector measurement technique. (a) SA with 120 μL $Cu_{3-x}P$ solution drop-casted onto a side-polished fiber. (b) SA with 240 μL $Cu_{3-x}P$ solution drop-casted onto the side-polished fiber (inset: optical image of the SA device). Scale bar: 100 μm

signal–noise rate was high at 75 dB, showing a high stability (Fig. 3(d)). Furthermore, the output laser pulses were operated stably, and no clear noise signal can be observed from the radio frequency (RF) spectrum with a wide frequency range (high at 1.5 GHz) in the inset of Fig. 3(d). The optical spectrum remained stable when the laser was continually run for over 6 h, further proving a high stability (Fig. 3(e)).

While drop-casting over 240 μL of $Cu_{3-x}P$ nanocrystals onto the side-polished fiber, the modulation depth and the extra saturable loss of the $Cu_{3-x}P$ nanocrystal-based SA significantly increased, thereby affording a typical Q-switched pulse generation from the cavity. Figures 4(a)–4(d) show the Q-switched pulse characteristics under the pump power of 300 mW. In Fig. 4(a), the central wavelength was 1560.9 nm, and the 3 dB spectral bandwidth was more than 1.2 nm. The smooth spectrum envelope indicates that the spectral component of the continuous wave was fully suppressed, thereby manifesting as a typical Q-switching state. The Q-switched pulse

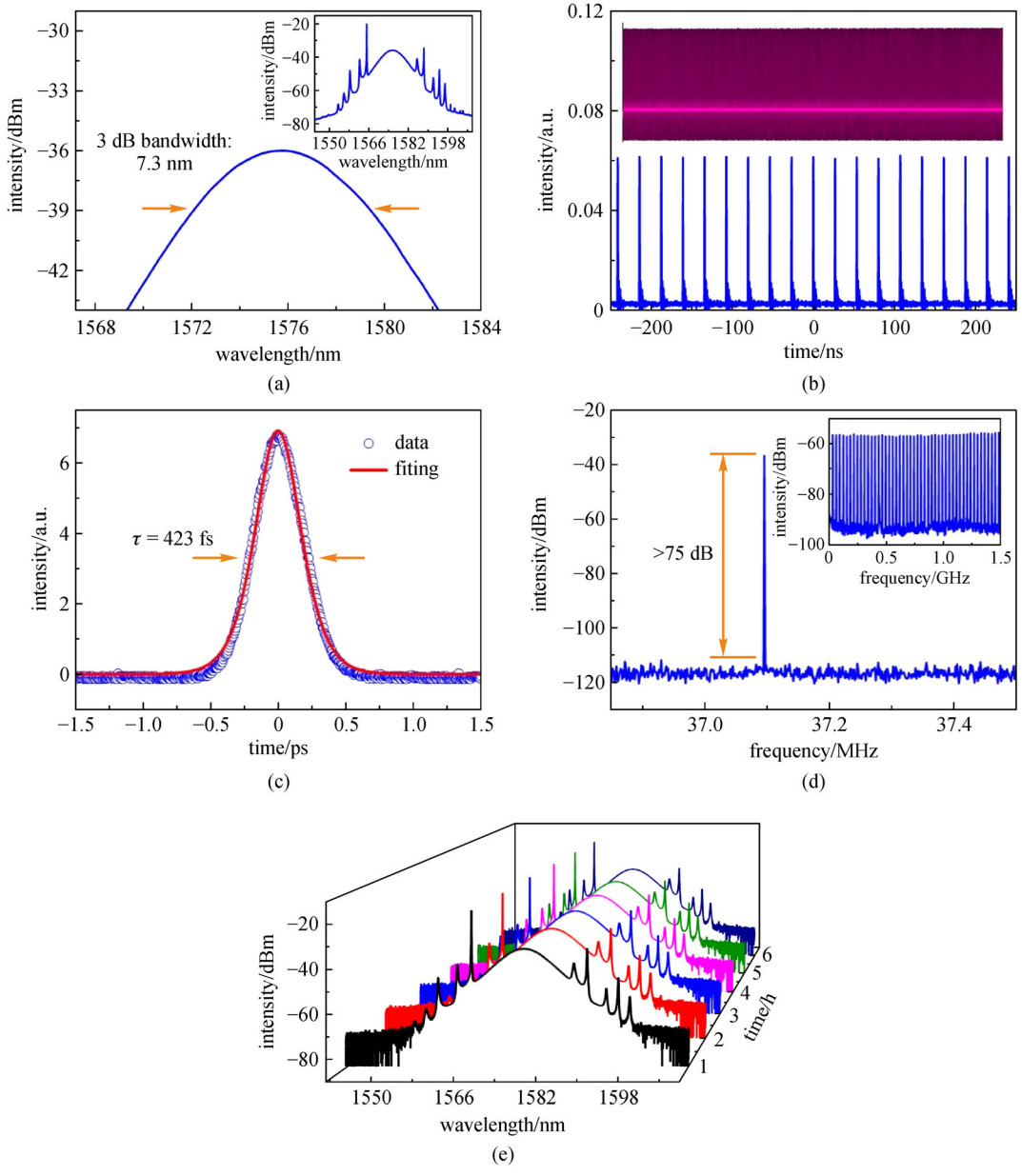

Fig. 3 Typical mode-locking characteristics. (a) Typical mode-locking optical spectrum (inset: zoom-in view of the optical spectrum). (b) Mode-locking pulse train (inset: pulse train over 1 ms). (c) Autocorrelation trace. (d) RF optical spectrum at the fundamental frequency (inset: wideband RF spectrum). (e) Long-term stability of the mode-locked laser by measuring the time-dependent optical spectra for up to 6 h

train in Fig. 4(b) had a relatively high repetition rate of 51.1 kHz and a corresponding time interval of 19.5 μs between adjacent pulses. No obvious amplitude modulation (at the fundamental or harmonic frequency of the cavity) was found on each individual Q-switched pulse envelope. In addition, each pulse had a symmetric intensity profile. The single pulse duration was approximately 1.78 μs (Fig. 4(c)). A RF spectrum was collected to study the operation stability of the Q-switched laser (Fig. 4(d)). The signal-to-noise ratio exceeded 47 dB, which is a quite high value compared to that of the Q-switched fiber lasers reported in other papers [27]. Furthermore, the RF spectrum with a wide span range (inset, Fig. 4(d)) revealed that in addition to the fundamental and harmonic frequencies, no any other frequency components can be observed, confirming that the resulting Q-switched pulses were highly stable. A few output parameters of the Q-switched laser, including repetition rate, pulse duration, output power, and single pulse energy, will be changed with the pump power increase. Figures 4(e) and 4(f) depict the change in these four output parameters with a pump power increase above 560 mW. Interestingly, the repetition rate almost linearly increased to 88 kHz with the pump power increase. By contrast, the pulse duration first dramatically decreased, then stabilized at around 1.3 μs (Fig. 4(e)). Meanwhile, the output power also gradually

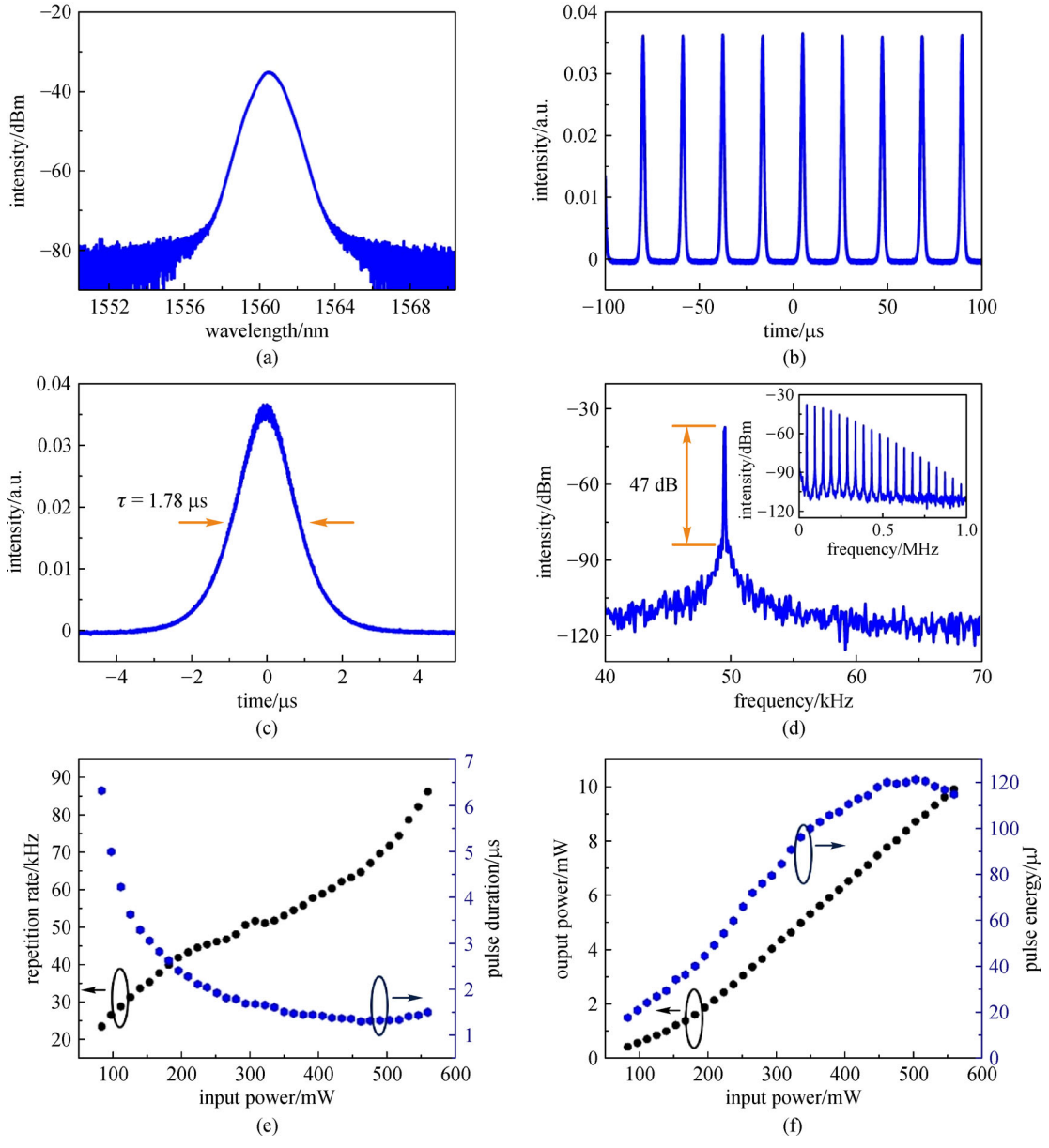

Fig. 4 Q-switched pulse output characteristics. (a) Optical spectrum. (b) Q-switched pulse train. (c) Single Q-switched pulse. (d) Radiofrequency optical spectrum at the fundamental frequency (inset: wideband RF spectrum). (e) Pulse repetition rate and duration versus incident pump power. (f) Output power versus incident pump power

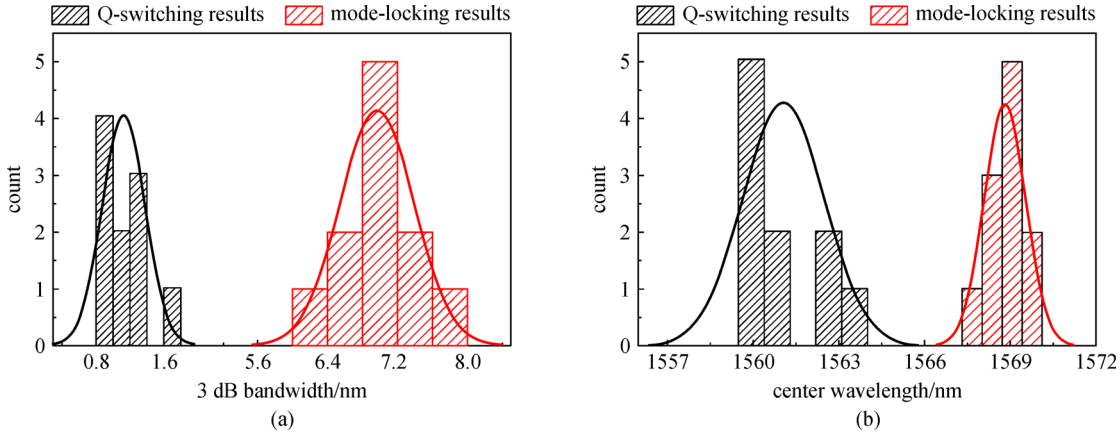

Fig. 5 Statistical distribution of the characteristics of the optical spectra collected from 10 pieces of $Cu_{3-x}P$-based Q-switched fiber lasers (black) and 11 pieces of $Cu_{3-x}P$-based mode-locked fiber lasers (red). (a) Statistical distribution of the 3 dB bandwidth and the corresponding Gauss-fitting results. (b) Statistical distribution of the central wavelength and the corresponding Gauss-fitting results

increased up to 10 mW with the pump power increase, suggesting that the Q-switched pulse, in principle, had a large pulse energy. The largest pulse energy was as high as 120 μJ under the pump power of 486 mW. The output quality of the laser remained very stable, and no obvious disturbance can be observed under any pump power (Fig. S2).

Apart from the excellent performance of the mode-locked and Q-switched lasers by 2D $Cu_{3-x}P$ SAs, the biggest advantages of the solution-phase SAs are easier processability and good repeatability, which make them suitable for large-scale industrial production. We fabricated 10 pieces of $Cu_{3-x}P$-based Q-switched SAs (240 μL $Cu_{3-x}P$ nanocrystals on the side-polished fiber) and 11 pieces of $Cu_{3-x}P$-based mode-locked SAs (120 μL $Cu_{3-x}P$ nanocrystals on the side-polished fiber). As expected, all pieces can effectively achieve Q-switched or mode-locked pulses. The optical spectra generated from these SAs under a pump power of 300 mW were recorded. Figures 5(a) and 5(b) summarize both the values of the 3 dB bandwidth and the center wavelength. The output spectra of the 2D $Cu_{3-x}P$-based mode-locked fiber laser normally have a 3 dB bandwidth of around 7 nm and a center wavelength at around 1569 nm, while those of the Q-switched fiber lasers had around 1.2 and 1561 nm, respectively. The slight difference in the output parameters in different SAs may be caused by the aggregation of the 2D nanocrystals during the drying process and the inhomogeneous distribution of the $Cu_{3-x}P$ nanocrystals in the fiber core area. Overall, the evaluation of over 20 $Cu_{3-x}P$-based SAs showed that the new kind of SA is very suitable for large-scale industrial production.

3 Conclusions

In this study, 2D $Cu_{3-x}P$ nanocrystals were employed as SA for ultrafast pulse generation. Both mode-locked and Q-switched pulses with high quality at around 1550 nm can be generated by tuning the amount of $Cu_{3-x}P$ nanocrystals. The 3 dB bandwidth of the mode-locked optical spectrum was as broad as 7.3 nm, and the corresponding pulse duration was 423 fs. The repetition rate of the Q-switched pulses was higher than 80 kHz. Furthermore, the largest pulse energy was more than 120 μJ. All fabricated SA devices (i.e., over 20 devices) can generate stable mode-locked and Q-switched pulses with similar characteristics, indicating that 2D nanocrystals have good reproducibility for fabricating SA devices in a large scale. Our work suggests that heavily doped colloidal plasmonic nanocrystals in the solution phase are promising and effective SAs for ultra-short or high-power pulse generation and other nonlinear photonic applications.

Acknowledgements We acknowledge the support from the National Key Research & Development Program (No. 2016YFA0201902), Shenzhen Nanshan District Pilotage Team Program (No. LHTD20170006) and Australian Research Council (ARC, FT150100450, IH150100006, and CE170100039). B.S. acknowledges the funding support from China Postdoctoral Science Foundation Grant (No. 217M622758). This work was performed in part at the Melbourne Centre for Nanofabrication (MCN) in the Victorian Node of the Australian National Fabrication Facility (ANFF).

References

1. Martinez A, Sun Z. Nanotube and graphene saturable absorbers for fibre lasers. Nature Photonics, 2013, 7(11): 842–845
2. Haus H A. Mode-locking of lasers. IEEE Journal of Selected Topics in Quantum Electronics, 2000, 6(6): 1173–1185
3. Keller U, Weingarten K J, Kartner F X, Kopf D, Braun B, Jung I D, Fluck R, Honninger C, Matuschek N, Der Au J A. Semiconductor saturable absorber mirrors (SESAM's) for femtosecond to nanosecond pulse generation in solid-state lasers. IEEE Journal of Selected Topics in Quantum Electronics, 1996, 2(3): 435–453
4. Autere A, Jussila H, Dai Y, Wang Y, Lipsanen H, Sun Z. Nonlinear optics with 2D layered materials. Advanced Materials, 2018, 30

(24): 1705963
5. Sun Z, Martinez A, Wang F. Optical modulators with 2D layered materials. Nature Photonics, 2016, 10(4): 227–238
6. Bao Q, Zhang H, Wang Y, Ni Z, Yan Y, Shen Z X, Loh K P, Tang D Y. Atomic-layer graphene as a saturable absorber for ultrafast pulsed lasers. Advanced Functional Materials, 2009, 19(19): 3077–3083
7. Shi H, Yan R, Bertolazzi S, Brivio J, Gao B, Kis A, Jena D, Xing H G, Huang L. Exciton dynamics in suspended monolayer and few-layer MoS_2 2D crystals. ACS Nano, 2013, 7(2): 1072–1080
8. Woodward R I, Kelleher E J. 2D saturable absorbers for fibre lasers. Applied Sciences, 2015, 5(4): 1440–1456
9. Martinez A, Yamashita S. 10 GHz fundamental mode fiber laser using a graphene saturable absorber. Applied Physics Letters, 2012, 101(4): 041118
10. Liu W, Pang L, Han H, Liu M, Lei M, Fang S, Teng H, Wei Z. Tungsten disulfide saturable absorbers for 67 fs mode-locked erbium-doped fiber lasers. Optics Express, 2017, 25(3): 2950–2959
11. Jin X, Hu G, Zhang M, Hu Y, Albrow-Owen T, Howe R C T, Wu T C, Wu Q, Zheng Z, Hasan T. 102 fs pulse generation from a long-term stable, inkjet-printed black phosphorus-mode-locked fiber laser. Optics Express, 2018, 26(10): 12506–12513
12. Jiang T, Yin K, Wang C, You J, Ouyang H, Miao R, Zhang C, Wei K, Li H, Chen H, Zhang R, Zheng X, Xu Z, Cheng X, Zhang H. Ultrafast fiber lasers mode-locked by two-dimensional materials: review and prospect. Photonics Research, 2020, 8(1): 78–90
13. Li P, Chen Y, Yang T, Wang Z, Lin H, Xu Y, Li L, Mu H, Shivananju B N, Zhang Y, Zhang Q, Pan A, Li S, Tang D, Jia B, Zhang H, Bao Q. Two-dimensional $CH_3NH_3PbI_3$ perovskite nanosheets for ultrafast pulsed fiber lasers. ACS Applied Materials & Interfaces, 2017, 9(14): 12759–12765
14. Ge Y, Zhu Z, Xu Y, Chen Y, Chen S, Liang Z, Song Y, Zou Y, Zeng H, Xu S, Zhang H, Fan D. Broadband nonlinear photoresponse of 2D TiS_2 for ultrashort pulse generation and all-optical thresholding devices. Advanced Optical Materials, 2018, 6(4): 1701166
15. Guo B, Wang S H, Wu Z X, Wang Z X, Wang D H, Huang H, Zhang F, Ge Y Q, Zhang H. Sub-200 fs soliton mode-locked fiber laser based on bismuthene saturable absorber. Optics Express, 2018, 26 (18): 22750–22760
16. Kou L Z, Tan X, Ma Y D, Tahini H, Zhou L J, Sun Z Q, Du A J, Chen C F, Smith S C. Tetragonal bismuth bilayer: a stable and robust quantum spin hall insulator. 2D Materials, 2015, 4: 045010
17. Comin A, Manna L. New materials for tunable plasmonic colloidal nanocrystals. Chemical Society Reviews, 2014, 43(11): 3957–3975
18. Liu X, Swihart M T. Heavily-doped colloidal semiconductor and metal oxide nanocrystals: an emerging new class of plasmonic nanomaterials. Chemical Society Reviews, 2014, 43(11): 3908–3920
19. Liu Z, Mu H, Xiao S, Wang R, Wang Z, Wang W, Wang Y, Zhu X, Lu K, Zhang H, Lee S T, Bao Q, Ma W. Pulsed lasers employing solution-processed plasmonic $Cu_{3-x}P$ colloidal nanocrystals. Advanced Materials, 2016, 28(18): 3535–3542
20. Scotognella F, Della Valle G, Srimath Kandada A R, Dorfs D, Zavelani-Rossi M, Conforti M, Miszta K, Comin A, Korobchevskaya K, Lanzani G, Manna L, Tassone F. Plasmon dynamics in colloidal $Cu_{2-x}Se$ nanocrystals. Nano Letters, 2011, 11(11): 4711–4717
21. Kriegel I, Jiang C, Rodríguez-Fernández J, Schaller R D, Talapin D V, da Como E, Feldmann J. Tuning the excitonic and plasmonic properties of copper chalcogenide nanocrystals. Journal of the American Chemical Society, 2012, 134(3): 1583–1590
22. Luther J M, Jain P K, Ewers T, Alivisatos A P. Localized surface plasmon resonances arising from free carriers in doped quantum dots. Nature Materials, 2011, 10(5): 361–366
23. Hamanaka Y, Hirose T, Yamada K, Kuzuya T. Plasmonic enhancement of third-order nonlinear optical susceptibilities in self-doped $Cu_{2-x}S$ nanoparticles. Optical Materials Express, 2016, 6(12): 3838–3848
24. Liu X, Guo Q, Qiu J. Emerging low-dimensional materials for nonlinear optics and ultrafast photonics. Advanced Materials, 2017, 29(14): 1605886
25. Henkes A E, Schaak R E. Trioctylphosphine: a general phosphorus source for the low-temperature conversion of metals into metal phosphides. Chemistry of Materials, 2007, 19(17): 4234–4242
26. Hsu S W, Ngo C, Tao A R. Tunable and directional plasmonic coupling within semiconductor nanodisk assemblies. Nano Letters, 2014, 14(5): 2372–2380
27. Popa D, Sun Z, Hasan T, Torrisi F, Wang F, Ferrari A C. Graphene Q-switched, tunable fiber laser. Applied Physics Letters, 2011, 98 (7): 073106

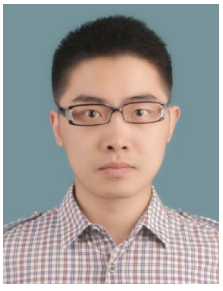

Haoran Mu is currently a Ph.D. candidate at Department of Materials Science and Engineering, Monash University, Australia. His research interest focuses on atomic-scale nonlinear photonics and applications and the realization of all-optical switches and modulations. He has published 19 papers with 9 papers of the first or co-first author.

Guanyu Liu is a postdoctoral researcher at Institute of Photonics Technology at Jinan University, China. He received his B.S. degree in Physics (2011) from Sun Yet-Sen University, China and his M.S. degree in Optics from Peking University (2014), China. He obtained his Ph.D. degree in Electronic Science and Technology from Peking University (2019), China. His current research focuses on ultrafast lasers and optoelectronic devices based on two-dimensional materials.

Qiaoliang Bao received his Ph.D. degree (2007) from Wuhan University, China. He worked as postdoctoral fellow at Nanyang Technological University and National University of Singapore, Singapore from 2007 to 2012. He was appointed as an associate professor at Department of Materials Science and Engineering, Monash University, Australia in 2016. His research

interests include photonics and optoelectronics based on two-dimensional materials with special focus on the effect of confined-space light-matter interactions. He has authored or coauthored more than 200 peer-reviewed journal articles with more than 17000 total citations and an h-index of 58. He was listed as Highly Cited (HiCi) researcher by Clarivate Analytics in 2018 and 2019.

Supporting Information

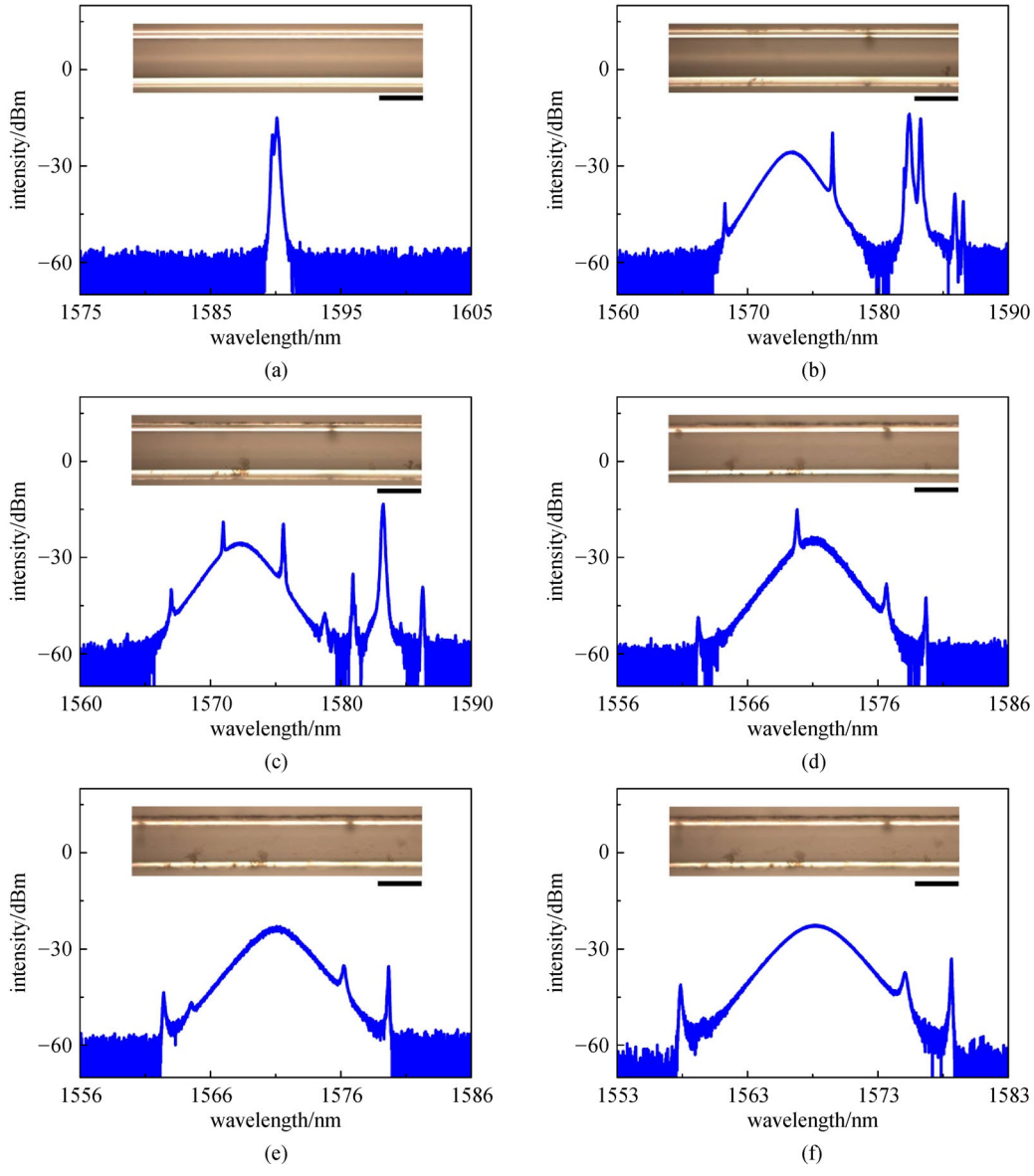

Fig. S1 Evolution of output optical spectra while using different amounts of $Cu_{3-x}P$ solution to prepare SA. (a) Brand new fiber without $Cu_{3-x}P$ nanocrystals. (b) 40 μL. (c) 60 μL. (d) 80 μL. (e) 100 μL. (f) 120 μL. All laser experiments were performed under the same condition of intra-cavity polarization state and pump power. Inset: optical images of the side-polished optical fibers (a) without or (b)–(f) with 2D $Cu_{3-x}P$ nanocrystals. Scale bar: 100 μm

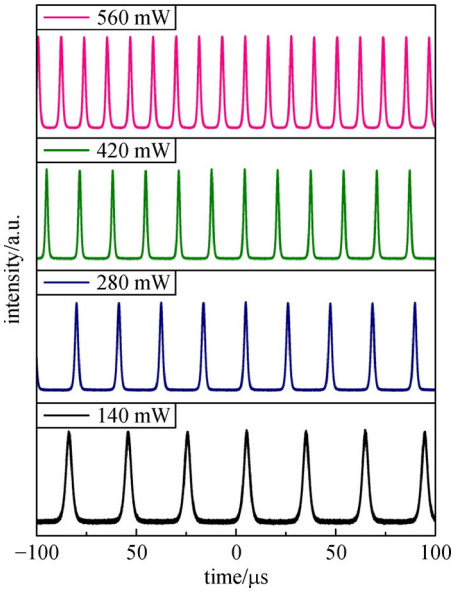

Fig. S2 Q-switched pulse trains obtained at different pump powers